Supporting Information

A Mononuclear Nonheme Manganese(III)-Aqua Complex as a New Active Oxidant in Hydrogen Atom Transfer Reactions

Muniyandi Sankaralingam,[†] Yong-Min Lee,[†] Deepika G. Karmalkar,[†] Wonwoo Nam,*[,†] and Shunichi Fukuzumi*[,†,‡]

[†]*Department of Chemistry and Nano Science, Ewha Womans University, Seoul 03760, Korea*

[‡]*Faculty of Science and Engineering, SENTAN, Japan Science and Technology Agency (JST), Meijo University, Nagoya, Aichi 468-0073, Japan*

E-mail: wwnam@ewha.ac.kr; fukuzumi@chem.eng.osaka-u.ac.jp

Table of Contents

Experimental Section

Materials. Commercially available chemicals were used without further purification unless otherwise indicated. Solvents were dried according to published procedures and distilled under an Ar atmosphere prior to use.[S1] 8-Aminoquinoline, bromoacetyl bromide, dipicolylamine, sodium carbonate, trifluromethanesulfonic acid, manganese powder, 2,4-di-*tert*-butylphenol, 2,6-di-*tert*-butyl-4-methylphenol, 2,6-di-*tert*-butyl-4-methoxyphenol, xanthene, 1,2,4-trimethoxybenzene, 3,4-dimethoxytoluene, *p*-cyano-*N*,*N*-dimethylaniline (*p*-CN-DMA), *p*-bromo-*N*,*N*-dimethylaniline (*p*-Br-DMA), dibromoferrocene (Br_2Fc), diacetylferrocene (Ac_2Fc), decamethylferrocene ($Me_{10}Fc$), acetonitrile-d_3, chloroform-*d*, deuterated water (D_2O), sodium hydride, dimethylsulfoxide-d_6 (DMSO-d_6), aqueous formaldehyde, 4-(methylamino)benzonitrile, *p*-cyanopyridine and acetonitrile were purchased from Aldrich chemical Co. and were of the best available purity. $Mn^{II}(OTf)_2{\cdot}2CH_3CN$ was prepared by the literature method.[S2] The dpaq ligand (dpaq = 2-bis(pyridin-2-ylmethyl)]amino-*N*-quinolin-8-yl-acetamidate) was synthesized according to the published procedures.[S3] The $[(dpaq)Mn^{III}(OH)](OTf)$ complex was synthesized by mixing the stoichiometric amounts of the dpaq ligand and $Mn(OTf)_2$ in an air-saturated MeCN solution followed by the addition of triethylamine.[S4]

Instrumentation. UV-vis spectra were recorded on a Hewlett Packard 8453 diode array spectrophotometer equipped with a UNISOKU Scientific Instruments Cryostat USP-203A for low-temperature experiments or on a Hi-Tech Scientific (U.K.) SF-61 DX2 cryogenic stopped-flow spectrophotometer equipped with a Xe arc lamp and a KinetaScan diode array rapid scanning unit. ^{1}H NMR spectra were measured with a Bruker model digital AVANCE III 400 FT-NMR spectrometer. Electrospray ionization mass (ESI-MS) spectra were collected using Thermo Finnigan (San Jose, CA, USA) LCQTM Advantage MAX quadrupole ion trap instrument, by infusing samples directly into the source at 20 μL min^{-1} using a syringe pump. The spray voltage was set at 4.7 kV while the capillary temperature was maintained at 80 ^{o}C. EPR spectra were recorded at 77 K with use of JEOL X-band spectrometer (JES-FA100). The spin amount of the Mn^{II} produced in the reaction of $[(dpaq)Mn^{III}(OH_2)]^{2+}$ with 2,4-di-*tert*-butylphenol in MeCN at 298 K was determined by the double integration of the EPR signal at 77 K, which was compared with that obtained from $Mn(OTf)_2$ used as a reference. The *g* value was calibrated using the Mn^{2+} marker. The EPR spectra were recorded under non-saturating

microwave power conditions. The magnitude of modulation was chosen to optimize the resolution and the signal-to-noise (S/N) ratio of the observed spectra. The experimental parameters for EPR measurements by JES-FA100 were as follows: microwave frequency = 9.028 GHz, microwave power = 1.0 mW, modulation amplitude = 3.0 G, modulation frequency = 100 kHz and time constant = 0.03 s. The product analyses were performed with an Agilent 6890N gas chromatograph (GC) and a FOCUS DSQ (dual-stage quadrupole) mass spectrometer (Thermo Finnigan, Austin, TX, USA) interfaced with a Finnigan FOCUS gas chromatograph (GC-MS). Electrochemical measurements were performed on a CHI630B electrochemical analyzer (CH Instruments, Inc.) under Ar atmosphere in deaerated MeCN containing 0.10 M Bu_4NPF_6 ($TBAPF_6$) as a supporting electrolyte at 298 K. A conventional three-electrode cell was used with a platinum working electrode (surface area of 0.30 mm^2), a platinum wire used as a counter electrode and an Ag/Ag^+ electrode as a reference electrode. The measured potentials were recorded with respect to an Ag/Ag^+ (0.010 M) reference electrode. All potentials (vs. Ag/Ag^+) were converted to values versus SCE by adding 0.29 V.[S5]

Isolation of $[(dpaq)Mn^{III}(OH_2)]^{2+}$ (**1**). $[(dpaq)Mn^{III}(OH_2)]^{2+}$ complex was generated by adding trifluromethanesulfonic acid (HOTf; 1 equiv dissolved in MeCN) into the solution of $[(dpaq)Mn^{III}(OH)]^+$ (**2**) in MeCN at 298 K. Solid powder was isolated by diffusion of diethyl ether into an MeCN solution of **1**.

X-ray Structural Analysis. Green colored plate like single crystals of **1** suitable for X-ray analysis were obtained by slow diffusion of diethylether into an MeCN solution of **1**. Crystallographic data collections were carried out on a Bruker SMART AXS diffractometer equipped with a monochromator in the Mo Kα (λ = 0.71073 Å) incident beam. Single crystals of **1** were mounted on a glass fiber tip with epoxy cement. The diffraction data for **1** were collected at 296 K on a Bruker SMART AXS diffractometer equipped with a monochromator in the Mo Kα (λ = 0.71073 Å) incident beam. The CCD data were integrated and scaled using the Bruker-SAINT software package, and the structure was solved and refined using SHEXTL V6.12.[S6] Hydrogen atoms were located in the calculated positions. The crystallographic data and selected bond distances and angles for **1** are listed in Tables S1 and S2 (CCDC 1854620). These data can be obtained free of charge via www.ccdc.cam.ac.uk/data_request/cif (or from the Cambridge

Crystallographic Data Centre, 12, Union Road, Cambridge CB21EZ, UK; fax: (+44) 1223-336-033; or E-mail deposit@ccdc.cam.ac.uk).

Deuterated Substrate Synthesis. Deuterated substrates were synthesized by a modified literature method:[S7] [xanthene-d_2] Xanthene (0.50 g, 2.7 mmol) was reacted with NaH (0.20 g, 8.1 mmol) in DMSO-d_6 (3.0 mL) under an Ar atmosphere. The deep red solution was stirred at room temperature for 8 h and then quenched with D_2O (5.0 mL). The crude product was filtered and washed with copious amounts of distilled H_2O. Purity of >99% deuteration was confirmed by ^{1}H NMR. [2,6-Di-*tert*-butyl-4-methylphenol-*d*] 2,6-di-*tert*-butyl-4-methylphenol (0.13 g) was dissolved in DMSO-d_6 (3.0 mL) along with 0.010 g of NaH under N_2. The solution was stirred overnight and then quenched with 5.0 mL of D_2O. White precipitate was collected, washed with D_2O, and dried under vacuum. Purity of >95% deuteration was confirmed by ^{1}H NMR.

Kinetic Isotope Measurements. The oxidation of substrates (i.e., 2,4-di-*tert*-butylphenol, 4-methyl-2,6-di-*tert*-butylphenol and 4-methoxy-2,6-di-*tert*-butylphenol) by **1** were carried out in the presence of same concentration of H_2O and D_2O (1.4 M, 2.8 M or 5.6 M) in MeCN at 298 K. Similarly, the oxidation of 4-methoxy-2,6-di-*tert*-butylphenol by **2** was also carried out in the presence of same concentration of H_2O and D_2O (1.4 M or 2.8 M) in MeCN at 298 K.

Spectral Redox Titration for the Equilibrium Constant (K_{et}). Redox titration of electron-transfer from $[Fe^{II}(Me_2bpy)_3]^{2+}$ (Me_2bpy = 4,4'-dimethyl-2,2'-bipyridine) to **1** (0.05 mM) was examined in the various concentrations of $[Fe^{II}(Me_2bpy)_3]^{2+}$ (0.025 – 0.150 mM) in MeCN at 298 K using a Hewlett Packard 8453 photodiode array spectrometer with a quarts cuvette (path length = 10 mm). Typically, a deaerated MeCN solution of $[Fe^{II}(Me_2bpy)_3]^{2+}$ (0.025 – 0.150 mM) was added to a deaerated MeCN solution containing **1** (0.050 mM). The concentration of $[Fe^{III}(Me_2bpy)_3]^{3+}$ was determined from the decay of the absorption band at λ = 520 nm due to $[Fe^{II}(Me_2bpy)_3]^{2+}$ ($\varepsilon_1 = 4.2 \times 10^3$ M^{-1} cm^{-1}) and **1** ($\varepsilon_2 = 2.5 \times 10^2$ M^{-1} cm^{-1}).

Determination of pK_a: The pK_a of **1** was determined by the acid-base titration with *p*-cyanopyridine (pK_a = 8.10).[S8] Titration of **1** (0.20 mM) with various concentrations of *p*-cyanopyridine (0.080 – 0.48 mM) was examined in MeCN at 298 K using a Hewlett Packard 8453 photodiode array spectrometer with a quarts cuvette (path length = 10 mm). Typically, a deaerated MeCN solution of *p*-cyanopyridine (0.080 – 0.48 mM) was added to a deaerated

MeCN solution containing **1** (0.20 mM). The concentration of $[Mn^{III}(OH)(dpaq)]^+$ was determined from the formation of the absorption band at λ = 385 nm ($\varepsilon = 3.3 \times 10^3$ M^{-1} cm^{-1}) due to $[Mn^{III}(OH)(dpaq)]^+$.

Kinetic Measurements. All the reactions were run in a 1-cm UV cuvette by monitoring UV-vis spectral changes of reaction solutions. First-order rate constants were determined under pseudo-first-order conditions (e.g., [substrate]/[**1** or **2**] > 10) by fitting the decay of absorption peaks due to complexes **1** and **2** in the oxidation reactions of phenol derivatives, hydrocarbons, and ferrocene derivatives by **1** and **2** in MeCN at 298 K. The first-order plots were linear for three or more half-lives with the correlation coefficient of ρ >0.99. In each case, it was confirmed that the rate constants derived from at least three independent measurements agreed within an experimental error of ±5%. The pseudo-first-order rate constants increased proportionally with the concentrations of substrates, from which second-order rate constants were determined.

Product Analysis. Products formed in the oxidation of substrates by **1** in MeCN at 298 K were analyzed by ^{1}H NMR, GC, and GC-MS. In GC quantitative analysis was performed by comparison against standard curves prepared with known authentic samples and using decane as an internal standard. In the reaction of **1** with 2,4-di-*tert*-butylphenol, the 3,3′,5,5′-tetra-*tert*-butylbiphenyl-2,2′-diol produced was analyzed by ^{1}H NMR and GC. The reaction of **1** with xanthene, formation of xanthone was confirmed by GC and GC-MS. The reaction of **1** with *p*-CN-DMA, the demethylated product (i.e., *p*-CN-Ph-$NHCH_3$) and formaldehyde was confirmed by the ^{1}H NMR spectroscopy compared with the authentic samples. The manganese products formed in the oxidation of substrates by **1** were analyzed by ESI-MS and EPR techniques. In all the reactions, Mn^{II} species was formed as a major product.

Table S1. Crystallographic Data and Refinements for **1**

	1
Empirical formula	$C_{25}H_{22}MnN_5O_8S_2F_6$
Formula weight	753.53
Temperature (K)	296(2)
Wavelength (Å)	0.71073
Crystal system/space group	orthorhombic, P 2ac 2ab
Unit cell dimensions	
a (Å)	10.049(4)
b (Å)	15.976(7)
c (Å)	18.860(8)
α (°)	90
β (°)	90
γ (°)	90
Volume ($Å^3$)	3028(2)
Z	4
Calculated density (g/cm^{-3})	1.653
Absorption coefficient (mm^{-1})	0.667
Reflections collected	21855
Absorption correction	multi-scan (T_{min} = 0.980, T_{max}= 0.936)
Independent reflections	5339
Goodness-of-fit on F^2	1.027
R [$F^2 > 2\text{sigma}(F^2)$]	0.0320
wR^2	0.0716

Table S2. Selected Bond Distances (Å) and Angles (º) for **1**

	1
Bond Distances (Å)	
Mn1-N1	2.106(3)
Mn1-N2	2.033(3)
Mn1-N3	2.249(3)
Mn1-N4	2.235(3)
Mn1-N5	1.920(3)
Mn1-O8	1.942(2)
Bond Angles (°)	
N1-Mn1-N2	164.90(12)
N1-Mn1-N3	78.66(12)
N1-Mn1-N4	77.75(11)
N1-Mn1-N5	84.19(12)
N2-Mn1-N3	103.69(12)
N2-Mn1-N4	100.70(12)
N2-Mn1-N5	80.82(12)
N3-Mn1-N4	155.61(11)
N3-Mn1-N5	92.28(13)
N4-Mn1-N5	91.43(12)
O8-Mn1-N1	96.41(11)
O8-Mn1-N2	98.55(11)
O8-Mn1-N3	88.50(11)
O8-Mn1-N4	88.04(11)
O8-Mn1-N5	179.09(13)

Table S3. One-Electron Oxidation Potentials (E_{ox}) of Electron Donors and Second-Order Rate Constants (k_{et}) of Electron Transfer from Electron Donors to **1** with Driving Force of Electron Transfer ($-\Delta G_{et}$) in MeCN at 298 K

electron donor	E_{ox} vs SCE,[a] V	k_{et}, M^{-1} s^{-1}	$-\Delta G_{et}$, eV
Br_2Fc	0.72	4.3×10^4	0.31
Ac_2Fc	0.83	1.4×10^4	0.20
p-Br-DMA	0.92	1.0×10^3	0.11
p-CN-DMA	1.15	24	–0.12

[a] Taken from the following references: (a) Yoon, H.; Morimoto, Y.; Lee, Y.-M.; Nam, W.; Fukuzumi, S. *Chem. Commun*. **2012**, *48*, 11187. (b) Park, J.; Morimoto, Y.; Lee, Y.-M.; You, Y.; Nam, W.; Fukuzumi, S. *Inorg. Chem.* **2011**, *50*, 11612.

Table S4. One-Electron Oxidation Potentials (E_{ox}) of Substrates and Second-Order Rate Constants (k_{ox}) of Oxidation of Substrates by **1** with Driving Force ($-\Delta G_{et}$) in MeCN at 298 K

electron donor	E_{ox} vs SCE,[a] V	k_{et}, M^{-1} s^{-1}	$-\Delta G_{et}$, eV
4-MeO-2,6-di-^{t}Bu-phenol	0.90	1.6×10^2	0.13
1,2,4-trimethoxybenzene	0.96	1.0×10^2	0.07
4-Me-2,6-di-^{t}Bu-phenol	1.24	3.0×10^{-1}	–0.21
3,4-di-methoxytoluene	1.33	2.1	–0.30
2,4-di-^{t}Bu-Phenol	1.46	2.9	–0.43

[a] Taken from the following references: (a) Osako, T.; Ohkubo, K.; Taki, M.; Tachi, Y.; Fukuzumi, S.; Itoh, S. *J. Am. Chem. Soc*. **2003**, *125*, 11027. (b) Ohkubo, K.; Mizushima, K.; Iwata, R.; Fukuzumi, S., *Chem. Sci.* **2011**, *2*, 715.

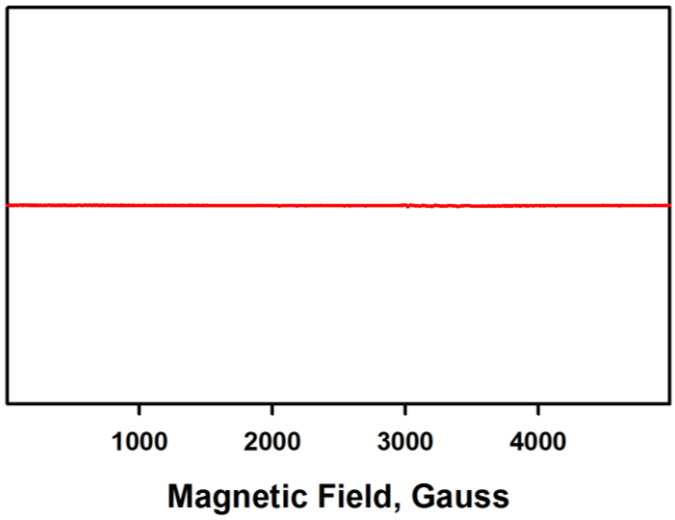

Figure S1. X-band EPR spectrum of $[(dpaq)Mn^{III}(OH_2)]^{2+}$ (**1**, 0.50 mM), which was generated by adding HOTf (0.50 mM) to $[(dpaq)Mn^{III}(OH)]^{+}$ (**2**, 0.50 mM) in MeCN at 298 K. Spectrum was recorded in MeCN at 77 K. We have performed the EPR measurements in the parallel mode for **1**. However, no signal due to **1** was observed in the parallel mode probably because of the large zero-field splitting that may result in broadening of the anticipated signal with parallel microwave polarization beyond detection.

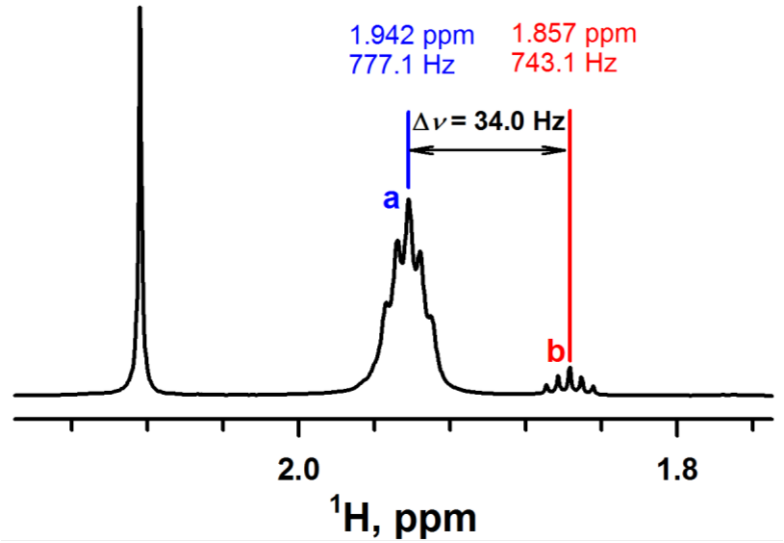

Figure S2. ^{1}H NMR (400 MHz) spectrum of $[(dpaq)Mn^{III}(OH_2)]^{2+}$ (**1**, 2.0 mM) recorded using the modified ^{1}H NMR method of Evans in CD_3CN at 298 K. A WILMAD® coaxial insert (sealed capillary) tube containing only the blank CD_3CN solvent was inserted into the normal NMR tubes containing **1** (2.0 mM) dissolved in CD_3CN. The chemical shift of the solvent peak (peak a) in the presence of the paramagnetic metal complex (**1**) was compared to that of the solvent peak (peak b) of the inner NMR tube. The magnetic moment was calculated using the following equation,

$$\mu = 0.0618(\Delta\nu T / 2fM)^{1/2}$$

where f is the oscillator frequency (MHz) of the superconducting spectrometer, T is the absolute temperature, M is the molar concentration of the metal ion, and $\Delta\nu$ is the difference in frequency (Hz) between the two reference signals. The ^{1}H NMR Evans method allowed us to determine magnetic moment of 4.92 μ_B for **1** in CD_3CN at 298 K, indicating that the **1** possesses an S = 2 spin state in CD_3CN solution.

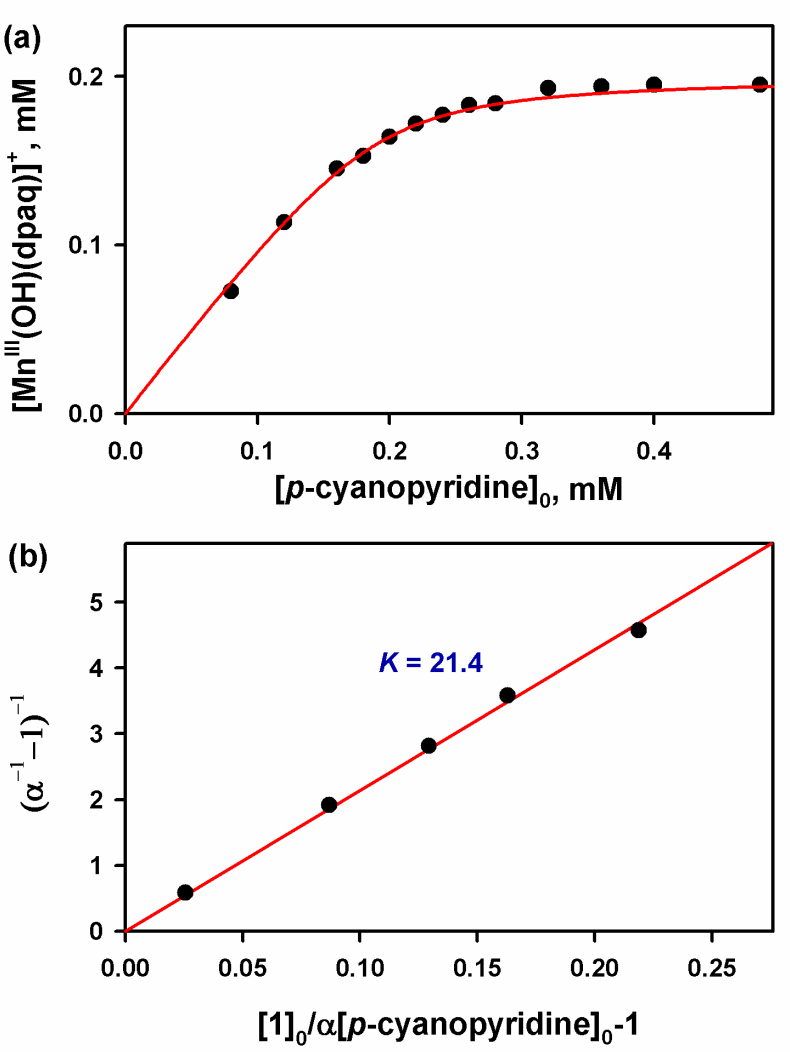

Figure S3. (a) Plot of concentration of **2** produced in the reaction of **1** (0.20 mM) with *p*-cyanopyridine (0.080 – 0.48 mM) in MeCN at 298 K. (b) Plot of $(\alpha^{-1} - 1)^{-1}$ against $[\mathbf{1}]_0/\alpha$[p-cyanopyridine]$_0$ – 1 (where α = $[[Mn^{III}(OH)(dpaq)]^+]/[p\text{-cyanopyridine}]_0$) to determine the equilibrium constant (K) for the reaction of **1** with *p*-cyanopyridine to an MeCN solution of **1** at 298 K.

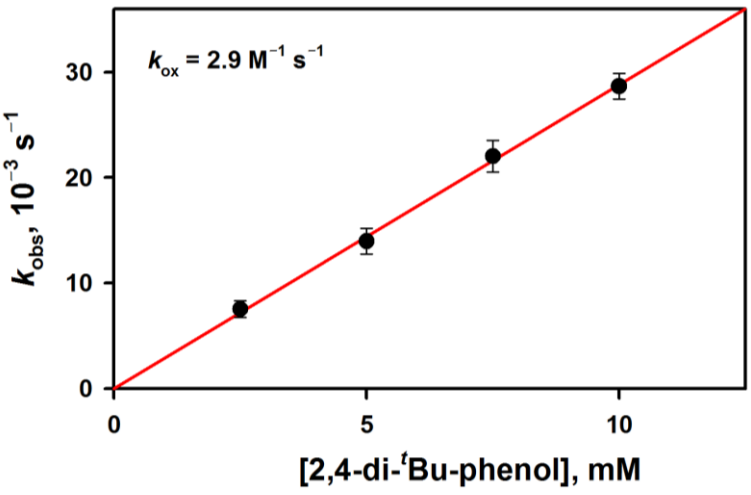

Figure S4. Plot of pseudo-first-order rate constants (k_{obs}) against the concentration of 2,4-di-*tert*-butylphenol to determine the second-order rate constants (k_{ox}) for the oxidation of 2,4-di-*tert*-butylphenol by **1** in MeCN at 298 K.

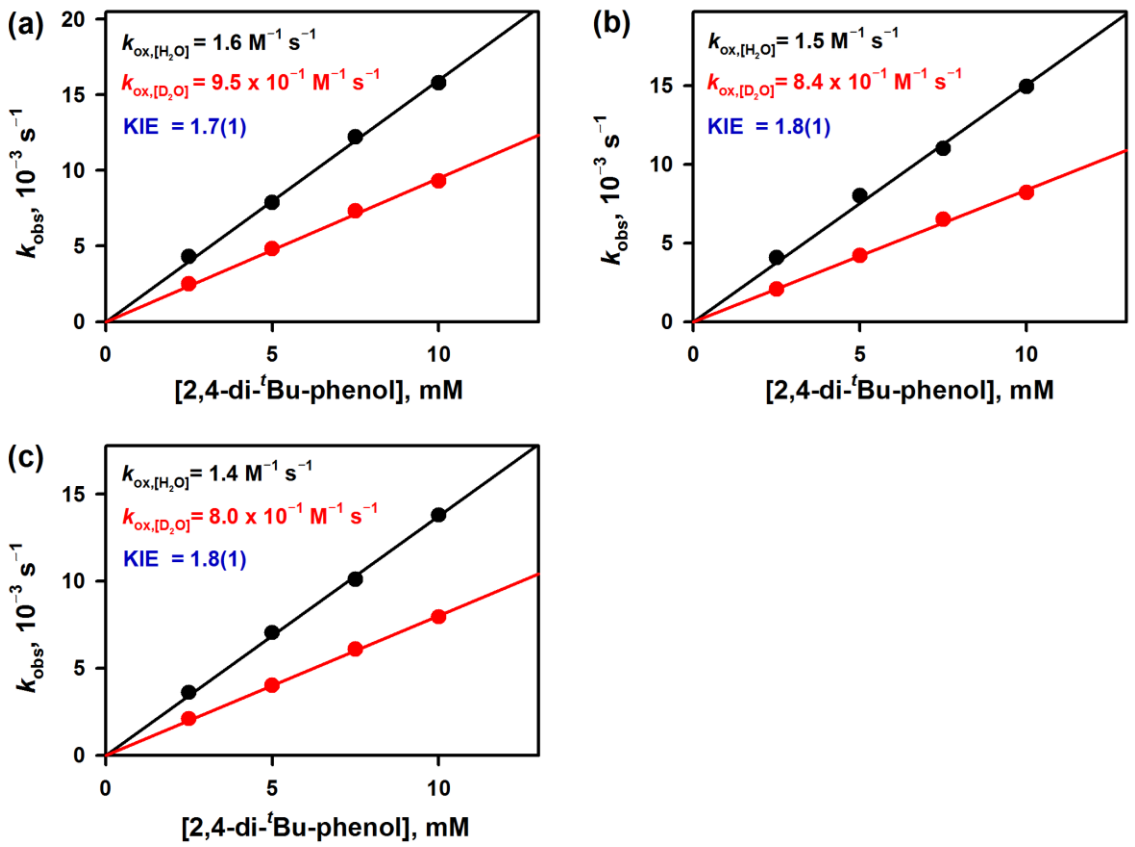

Figure S5. Plots of pseudo-first-order rate constants (k_{obs}) against the concentration of 2,4-di-*tert*-butylphenol obtained in the oxidation of 2,4-di-*tert*-butylphenol by **1** in the presence of H_2O and D_2O [(a) 2.8 M, (b) 4.2 M, and (c) 5.6 M] in MeCN at 298 K to determine the second-order rate constants (k_{ox}) and KIE values.

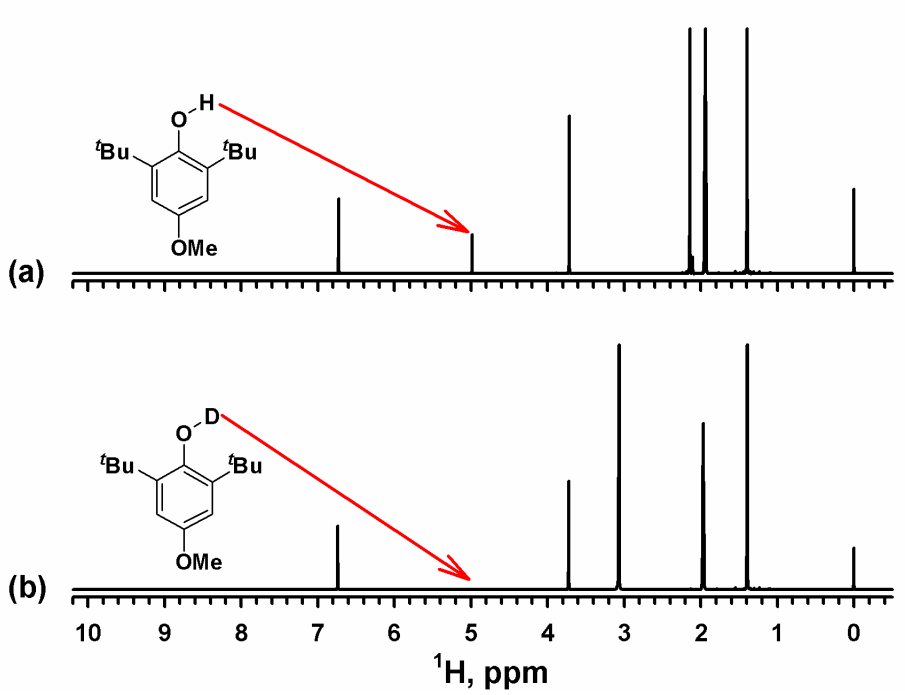

Figure S6. ^{1}H NMR spectra of the 2,6-di-*tert*-butyl-4-methoxyphenol (10 mM) in the (a) absence and (b) presence of D_2O (5.0 M) in CD_3CN at 298 K. The phenolic proton in 2,6-di-*tert*-butyl-4-methoxyphenol (10 mM) was exchanged completely with D of D_2O (5.0 M) within 5 min.

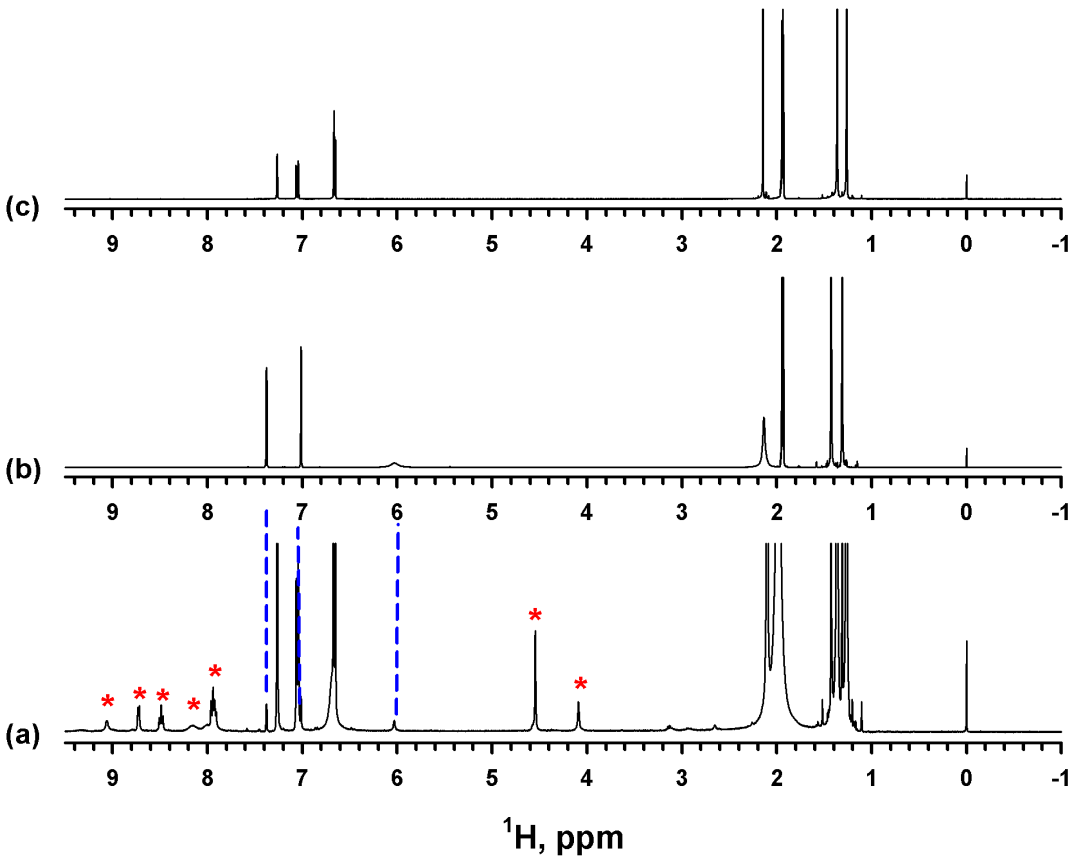

Figure S7. ^{1}H NMR spectra of (a) the reaction products and (b, c) the authentic reference samples [(b) 3,3′,5,5′-tetra-*tert*-butylbiphenyl-2,2′-diol and (c) 2,4-di-*tert*-butylphenol] in CD_3CN at 298 K. The reaction products were obtained in the oxidation of 2,4-di-*tert*-butylphenol (40 mM) by **1** (4.0 mM) in CD_3CN at 298 K. The peaks marked with * in (a) are from the dpaq ligand.

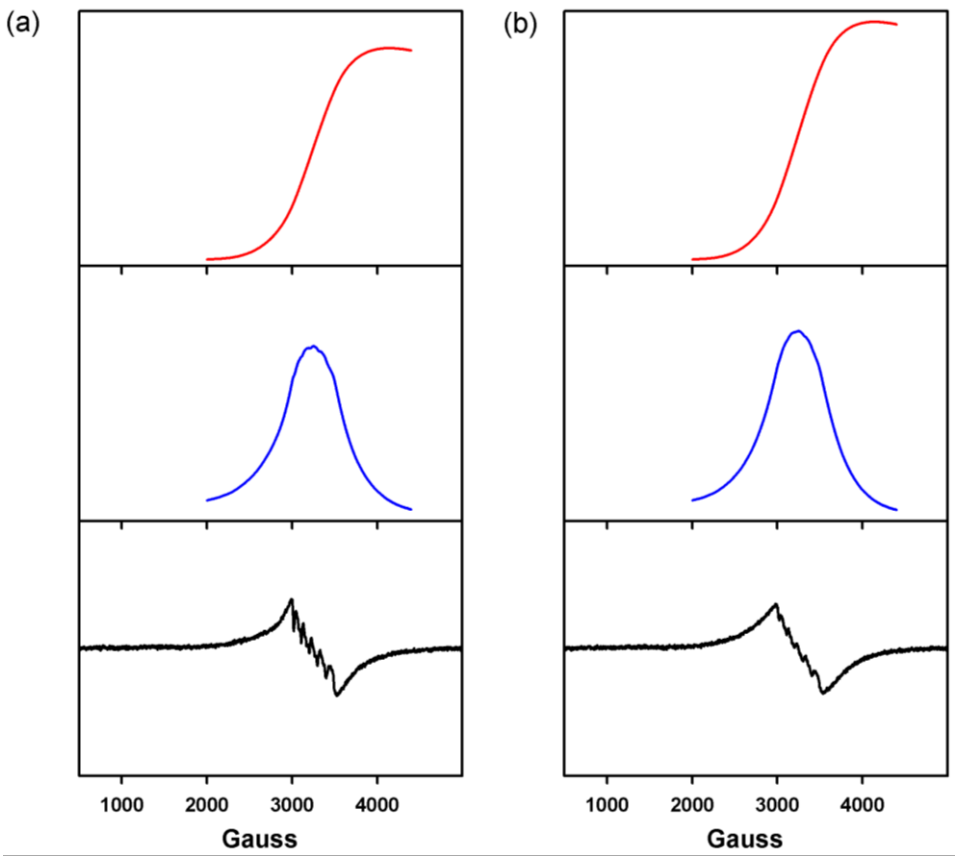

Figure S8. First derivative (black lines), integrated (blue lines) and doubly integrated (red lines) EPR spectra of (a) the reaction products and (b) $Mn^{II}(OTf)_2$ (0.50 mM) used as a reference. The reaction products were obtained in the oxidation of 2,4-di-*tert*-butylphenol (8.0 mM) by **1** (0.50 mM) in MeCN at 298 K. The spin amount of the Mn^{II} species produced was determined to be 90(3)%. Spectra were recorded in MeCN 77 K.

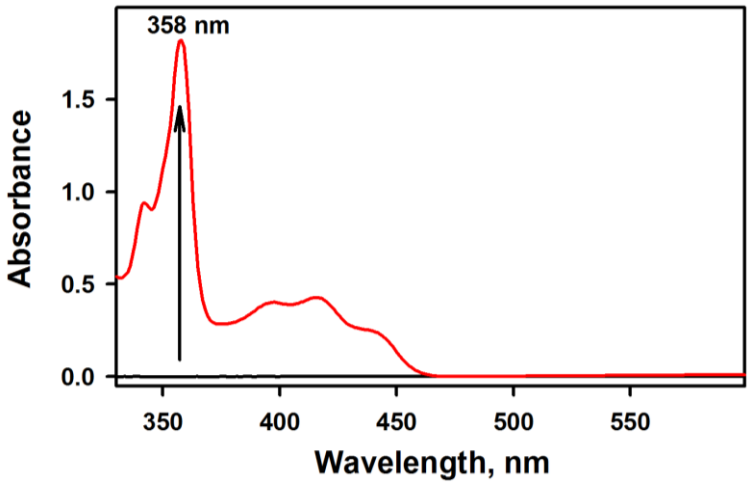

Figure S9. UV-vis spectral change observed upon addition of acridine (0.20 mM) to the reaction solution of the oxidation of 2,4-di-*tert*-butylphenol (8.0 mM) by **1** (0.20 mM) in MeCN at 298 K. The yield of the acridinium ion was determined to be 0.10 mM (50% based on the amount of **1** used).

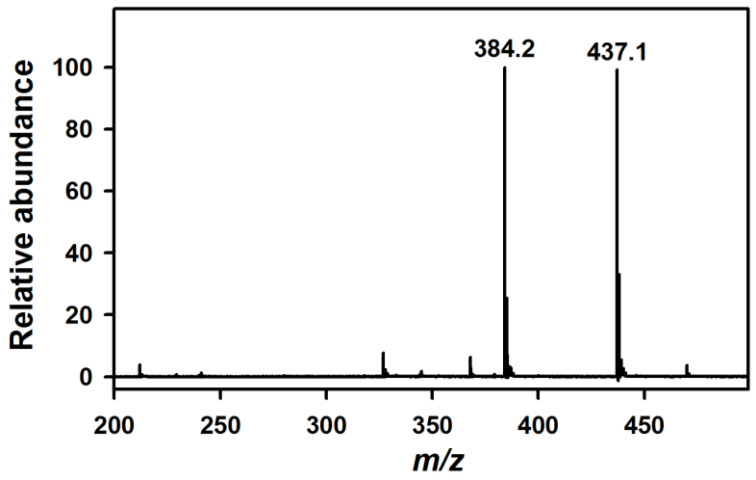

Figure S10. ESI-MS spectrum of the reaction solution of the oxidation of 2,4-di-*tert*-butylphenol by **1** in MeCN at 298 K. Peaks at *m/z* = 384.2 and 437.1 correspond to $[H\text{-dpaq}]^+$ (*calc. m/z* = 384.2) and $[Mn^{II}(dpaq)]^+$ (*calc. m/z* = 437.1), respectively.

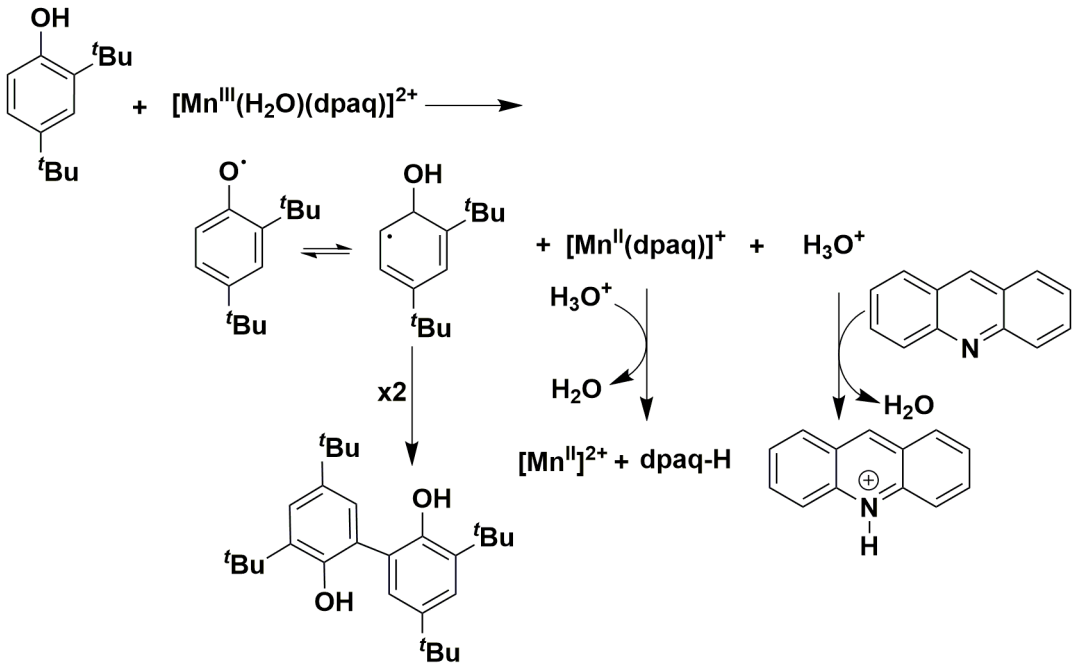

Figure S11. Reaction scheme for the oxidation of 2,4-di-*tert*-butylphenol by **1**.

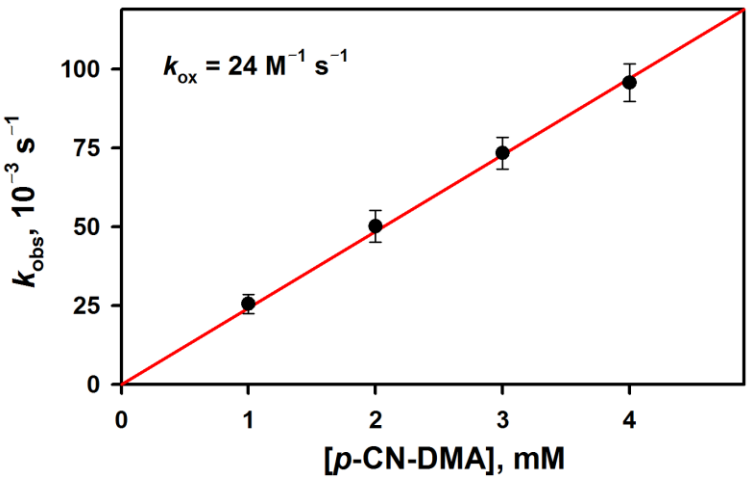

Figure S12. Plot of pseudo-first-order rate constants (k_{obs}) against *p*-CN-*N*,*N*-dimethylaniline (*p*-CN-DMA) concentration to determine the second-order rate constant (k_{ox}) for the oxidation of *p*-CN-DMA by **1** in MeCN at 298 K.

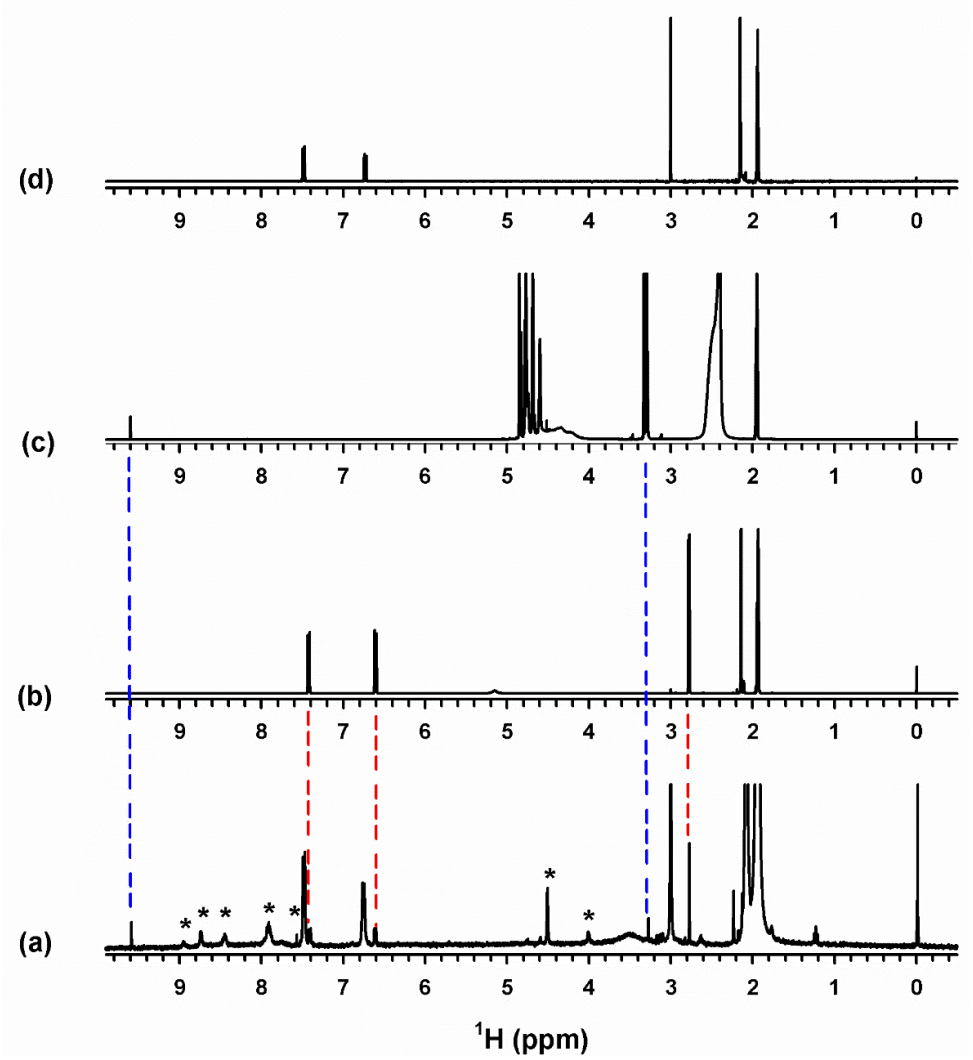

Figure S13. ^{1}H NMR spectra of (a) the reaction products and (b – d) the authentic reference samples [(b) *p*-CN-NH-CH_3-aniline, (c) aqueous formaldehyde, and (d) *p*-CN-DMA] in CD_3CN at 298 K. The reaction products were obtained in the oxidation of *p*-CN-DMA (5.0 mM) by **1** (2.0 mM) in CD_3CN at 298 K. The peaks marked with * in (a) are from the dpaq ligand.

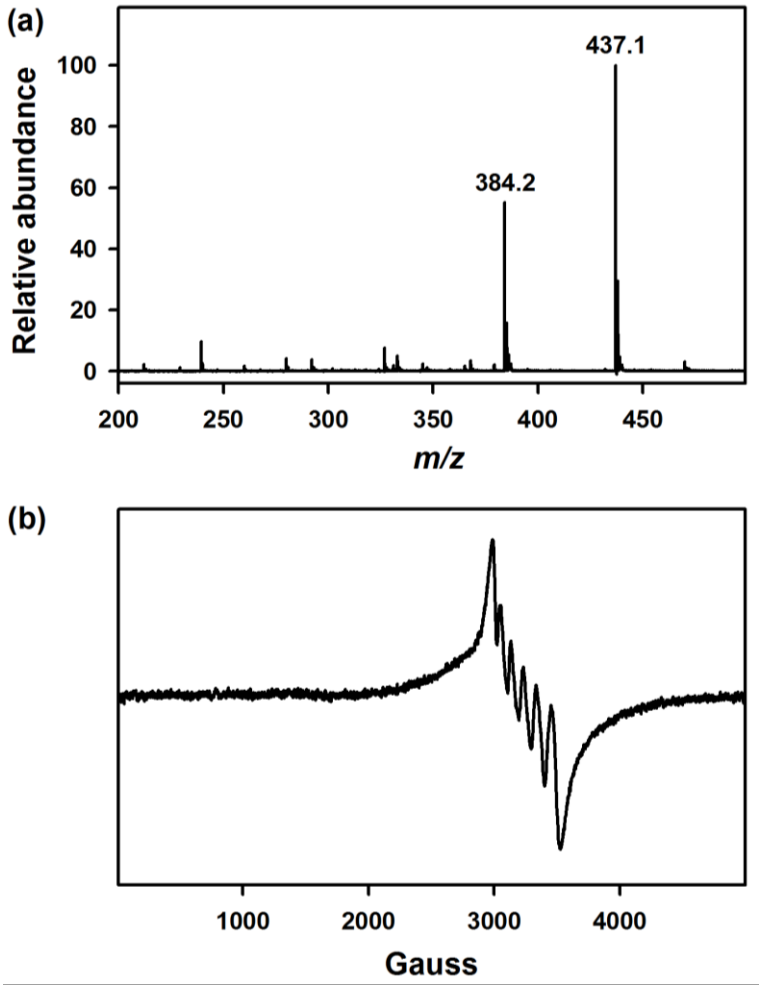

Figure S14. (a) ESI-MS spectrum of the reaction products obtained in the oxidation of *p*-CN-DMA by **1** in MeCN at 298 K. Peaks at *m/z* = 384.2 and 437.1 correspond to $[\text{H-dpaq}]^+$ (*calc.* *m/z* = 384.2) and $[\text{Mn}^{\text{II}}(\text{dpaq})]^+$ (*calc.* *m/z* = 437.1), respectively. (b) EPR spectrum of the reaction products obtained in the oxidation of *p*-CN-DMA by **1** in MeCN at 298 K. EPR spectrum was recorded at 77 K.

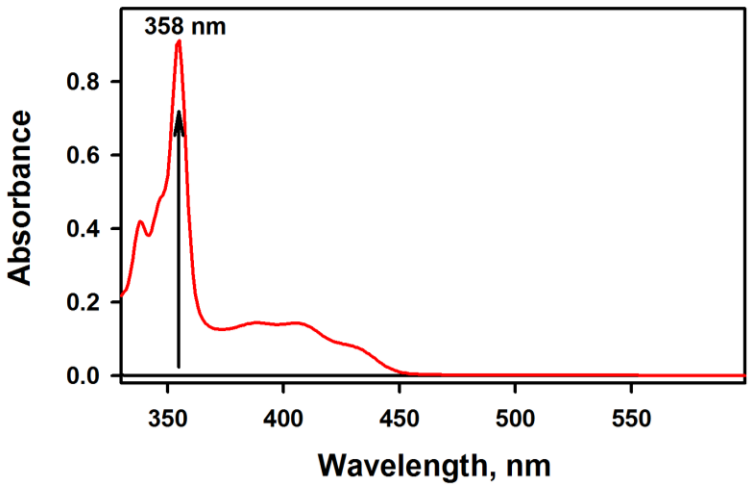

Figure S15. UV-vis spectral change observed upon addition of acridine (0.10 mM) to the reaction solution obtained in the oxidation of *p*-CN-DMA (2.0 mM) by **1** (0.10 mM) in MeCN at 298 K. The yield of the acridinium ion was determined to be 0.050 mM (50% based on the amount of **1** used).

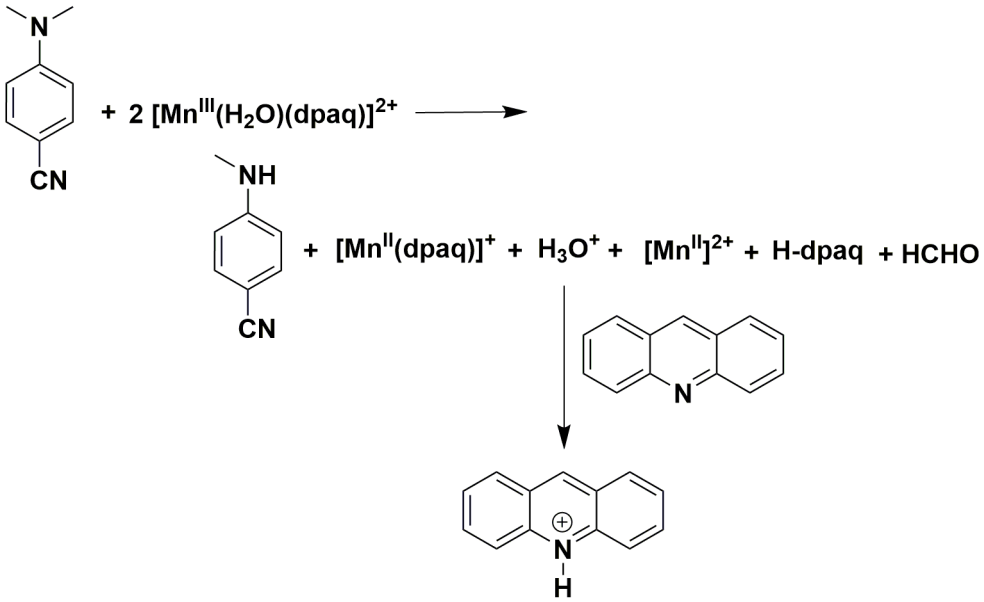

Figure S16. Reaction scheme showing the stoichiometry of the oxidation of *p*-CN-DMA by **1**.

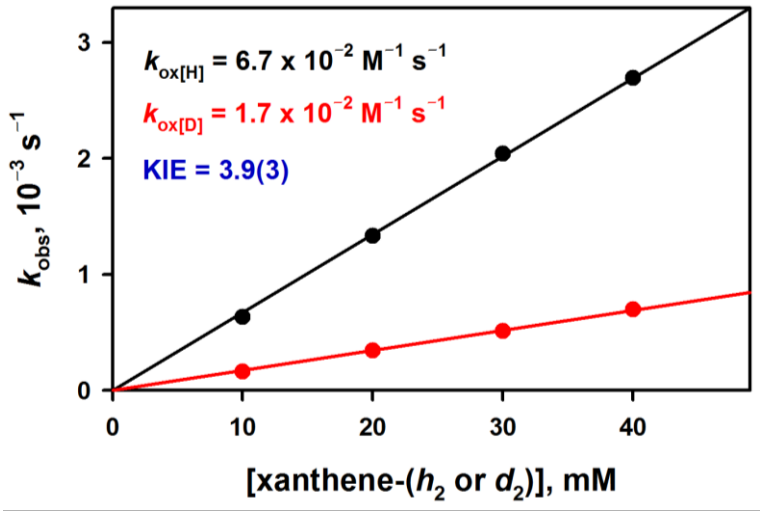

Figure S17. Plots of pseudo-first-order rate constants (k_{obs}) against substrate concentration obtained in the oxidation of xanthene-h_2 (black circle) and xanthene-d_2 (red circle) by **1** in MeCN at 298 K to determine the second-order rate constants (k_{ox}) and the KIE value.

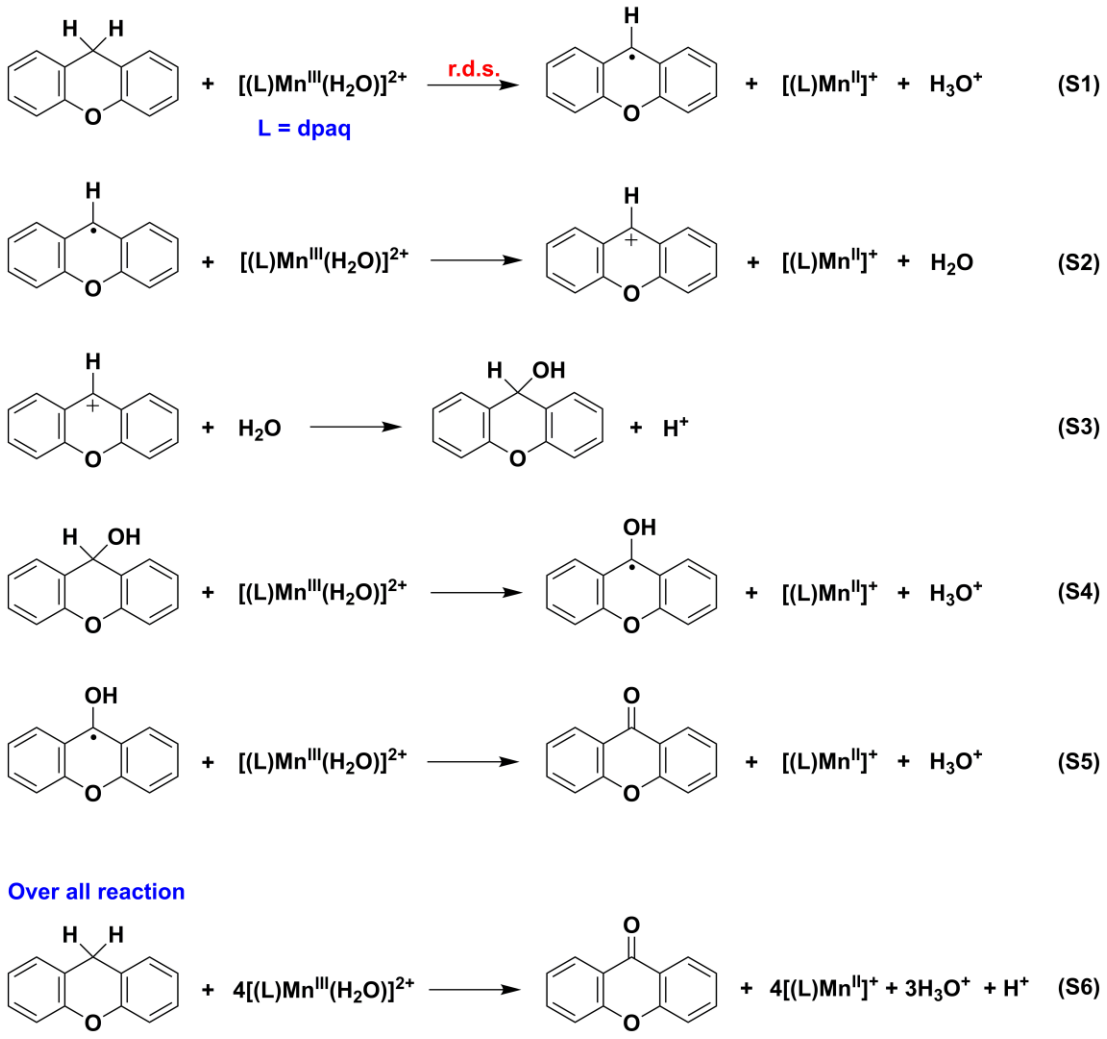

Figure S18. Overall reaction mechanism for the formation of xanthone in the oxidation reaction of xanthene by **1**.

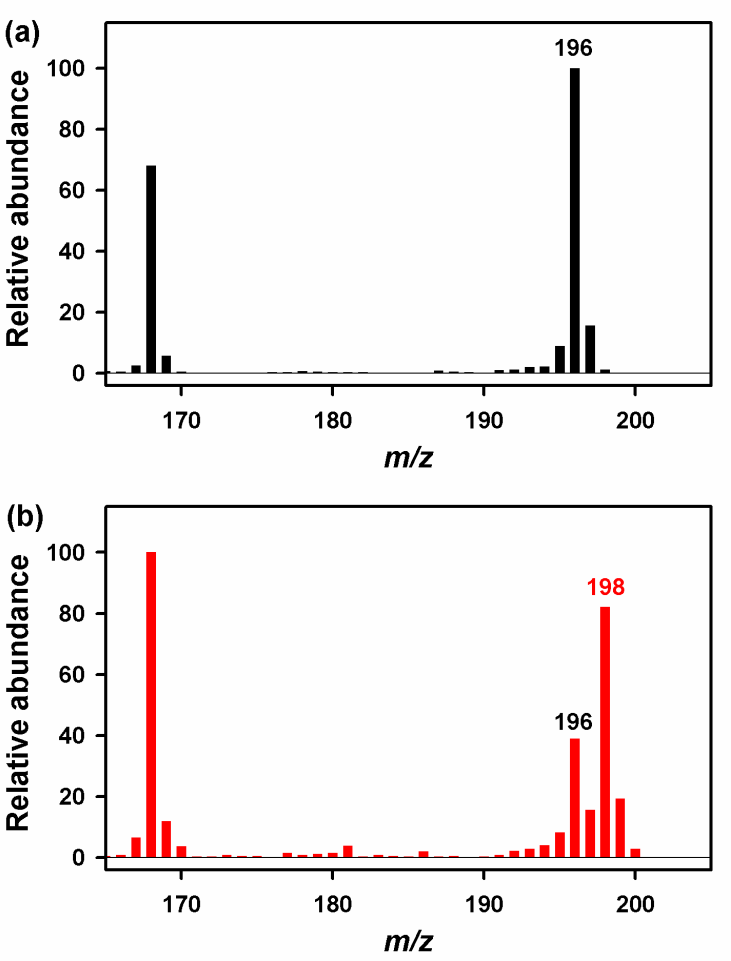

Figure S19. GC-MS spectra of (a) xanthone as an authentic reference and (b) xanthone produced in the oxidation of xanthene by **1** in the presence of $H_2{}^{18}O$ in MeCN 298 K.

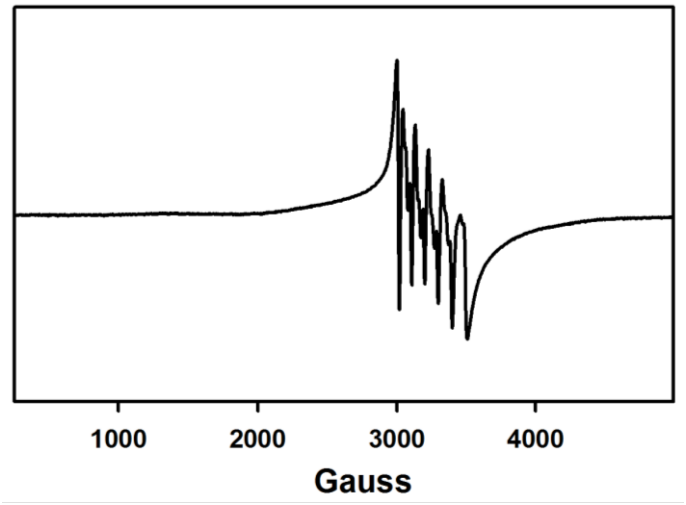

Figure S20. EPR spectrum of the reaction products obtained in the oxidation of xanthene by **1** in MeCN at 298 K. EPR spectrum was recorded at 77 K.

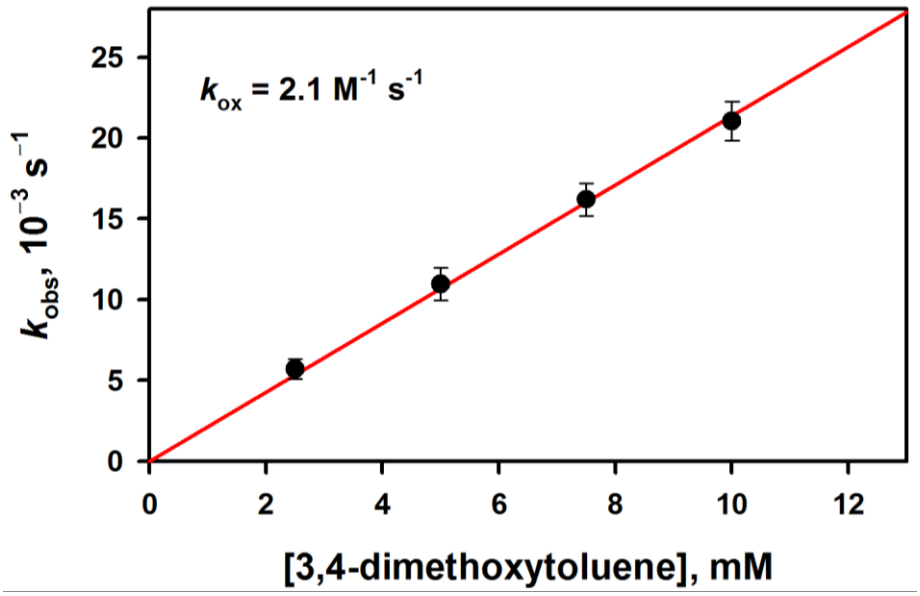

Figure S21. Plot of pseudo-first-order rate constants (k_{obs}) against concentration of 3,4-dimethoxytoluene obtained in the oxidation of 3,4-dimethoxytoluene by **1** in MeCN at 298 K to determine the second-order rate constant (k_{ox}).

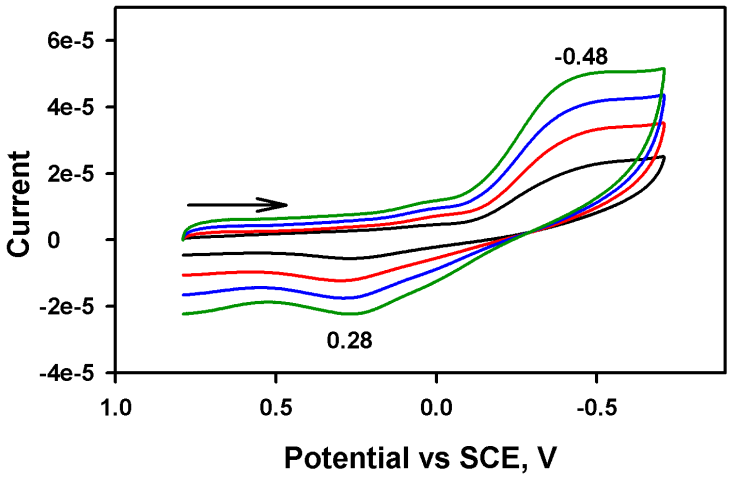

Figure S22. Cyclic voltammograms of $[(dpaq)Mn^{III}(OH)]^{+}$ (2.0 mM) with various scan rates [0.10 V s^{-1} (black line), 0.20 V s^{-1} (red line), 0.30 V s^{-1} (blue line), and 0.40 V s^{-1} (green line)] under argon atmosphere in deaerated MeCN containing $TBAPF_6$ (0.10 M) at 298 K.

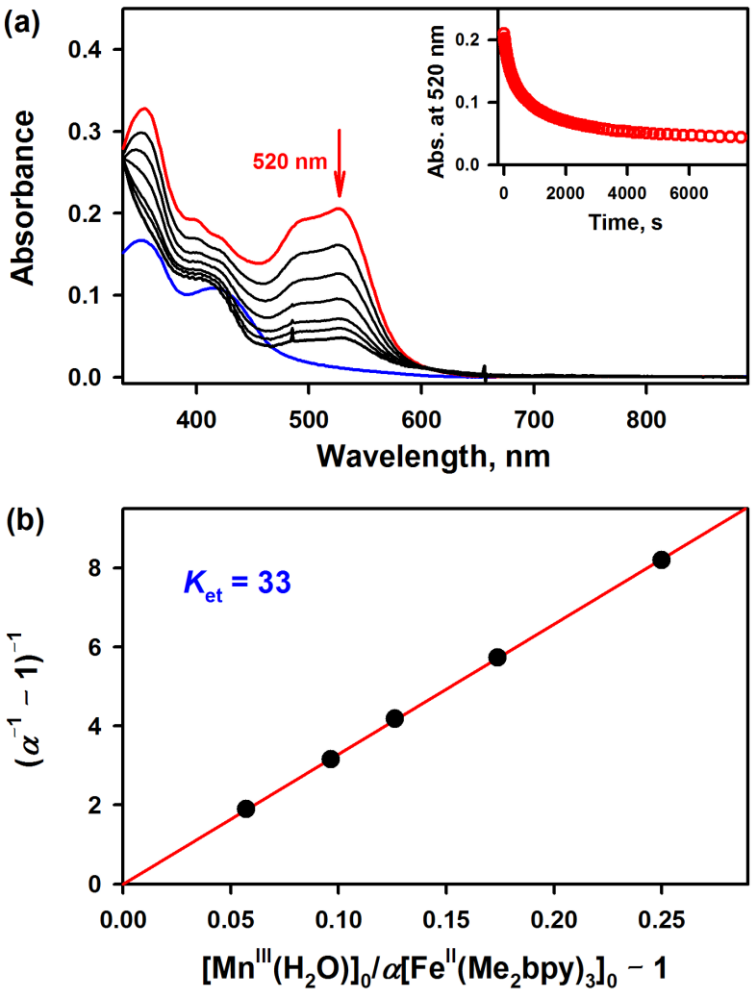

Figure S23. (a) UV-vis absorption spectral changes observed upon addition of $[Fe^{II}(Me_2bpy)_3]^{2+}$ (0.050 mM, red line) to **1** (0.050 mM, blue line) in MeCN at 298 K. Inset shows time profile monitoring the decay of the absorption peak at 520 nm due to $[Fe^{II}(Me_2bpy)_3]^{2+}$. (b) Plot of $(\alpha^{-1} - 1)^{-1}$ vs $[\mathbf{1}]_0/\alpha[[Fe^{II}(Me_2bpy)_3]^{2+}]_0 - 1$ (where $\alpha = [[Fe^{III}(Me_2bpy)_3]^{3+}]/[[Fe^{II}(Me_2bpy)_3]^{2+}]_0$) to determine the equilibrium constant (K_{et}) of electron transfer from $[Fe^{II}(Me_2bpy)_3]^{2+}$ to **1** upon addition of $[Fe^{II}(Me_2bpy)_3]^{2+}$ to an MeCN solution of **1** at 298 K.

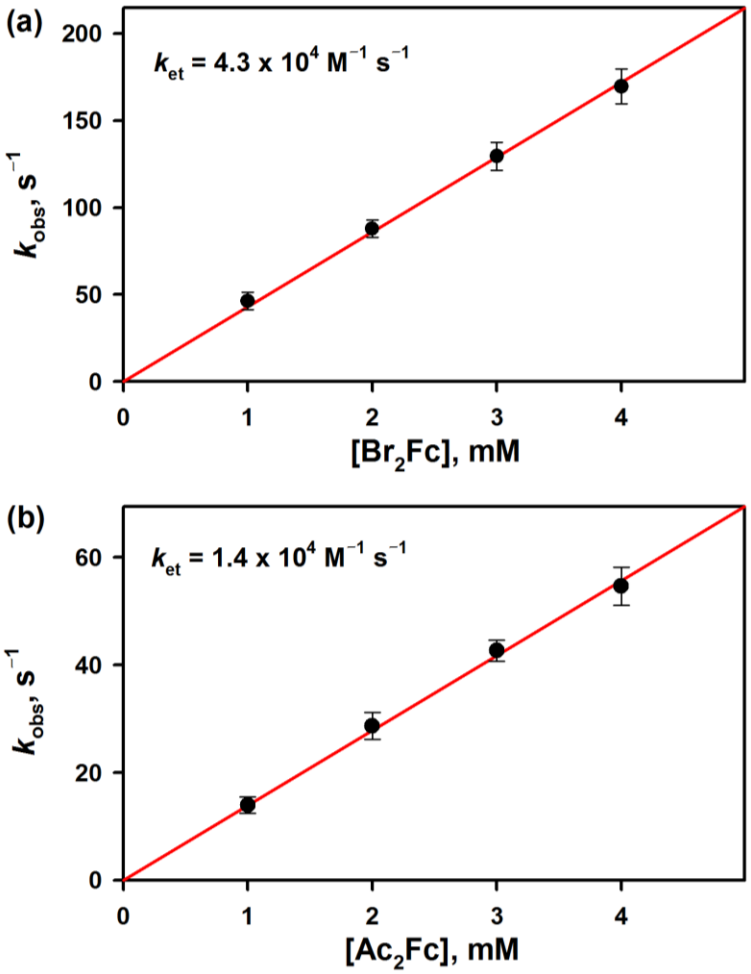

Figure S24. Plots of pseudo-first-order rate constants (k_{obs}) against concentration of one-electron donors obtained in the electron transfer reactions of **1** with one-electron donors [(a) Br_2Fc and (b) Ac_2Fc] in MeCN at 298 K to determine the second-order rate constants (k_{et}) of electron transfer from one-electron donors to **1**.

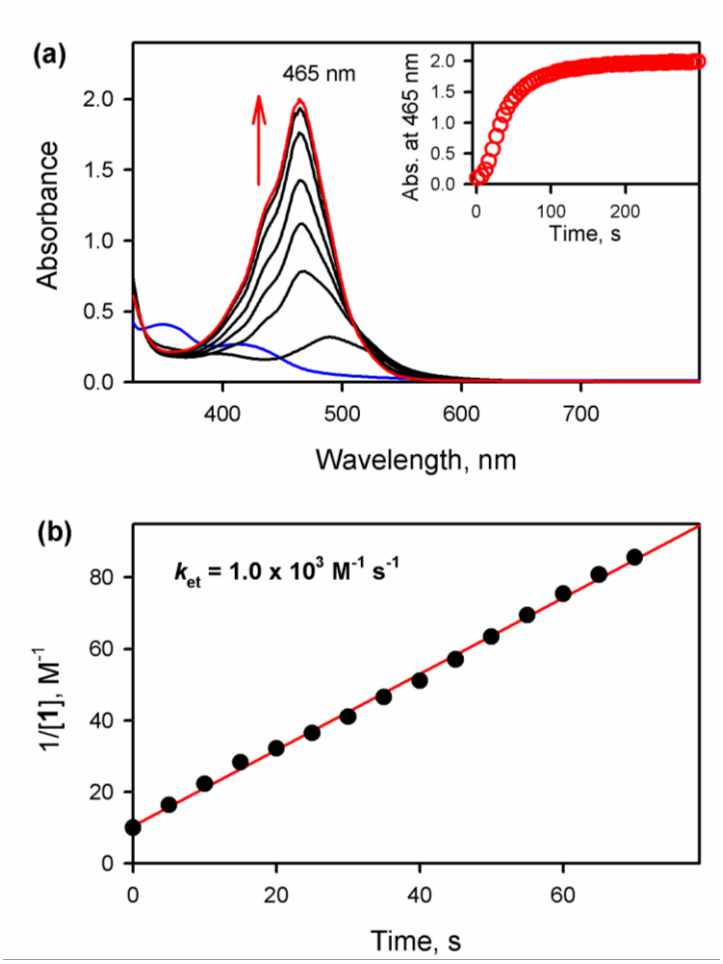

Figure S25. (a) UV-visible absorption spectral changes observed in the reaction of **1** (0.10 mM) with *p*-bromo-*N*,*N*-dimethylaniline (*p*-Br-DMA; 0.10 mM) in MeCN at 298 K. Inset shows time profile of the absorbance at 465 nm due to the formation of *p*-Br-DMA radical cation. (b) Second-order plot of 1/[**1**] against time for electron transfer from *p*-Br-DMA (0.10 mM) to **1** (0.10 mM) in MeCN at 298 K.

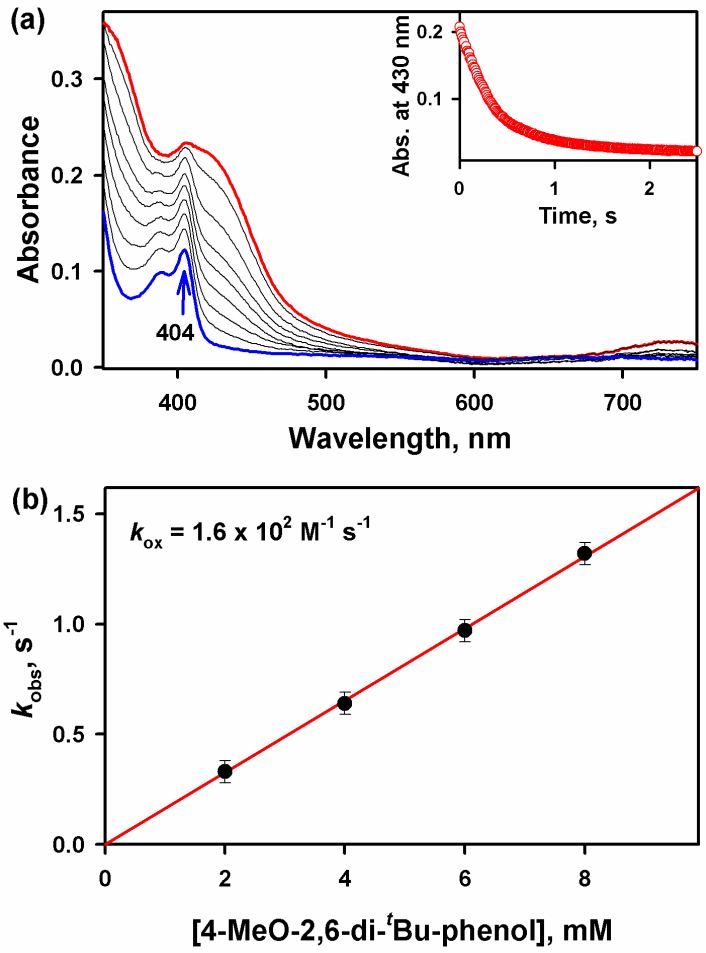

Figure S26. (a) UV-visible absorption spectral changes observed in the reaction of **1** (0.10 mM) with 4-methoxy-2,6-di-*tert*-butylphenol (8.0 mM) in MeCN at 298 K. Inset shows time profile of the decay of absorbance at 430 nm. The peak at 404 nm indicates the formation of the 4-methoxy-2,6-di-*tert*-butylphenoxyl radical, and phenoxyl radical was determined to be >80 % by molar absorption coefficient at 404 nm (ε = 1560 M^{-1} cm^{-1}). (b) Plot of pseudo-first-order rate constant (k_{obs}) against concentration of 4-methoxy-2,6-di-*tert*-butylphenol obtained in the oxidation of 4-methoxy-2,6-di-*tert*-butylphenol by **1** in MeCN at 298 K to determine the second-order rate constant (k_{ox}).

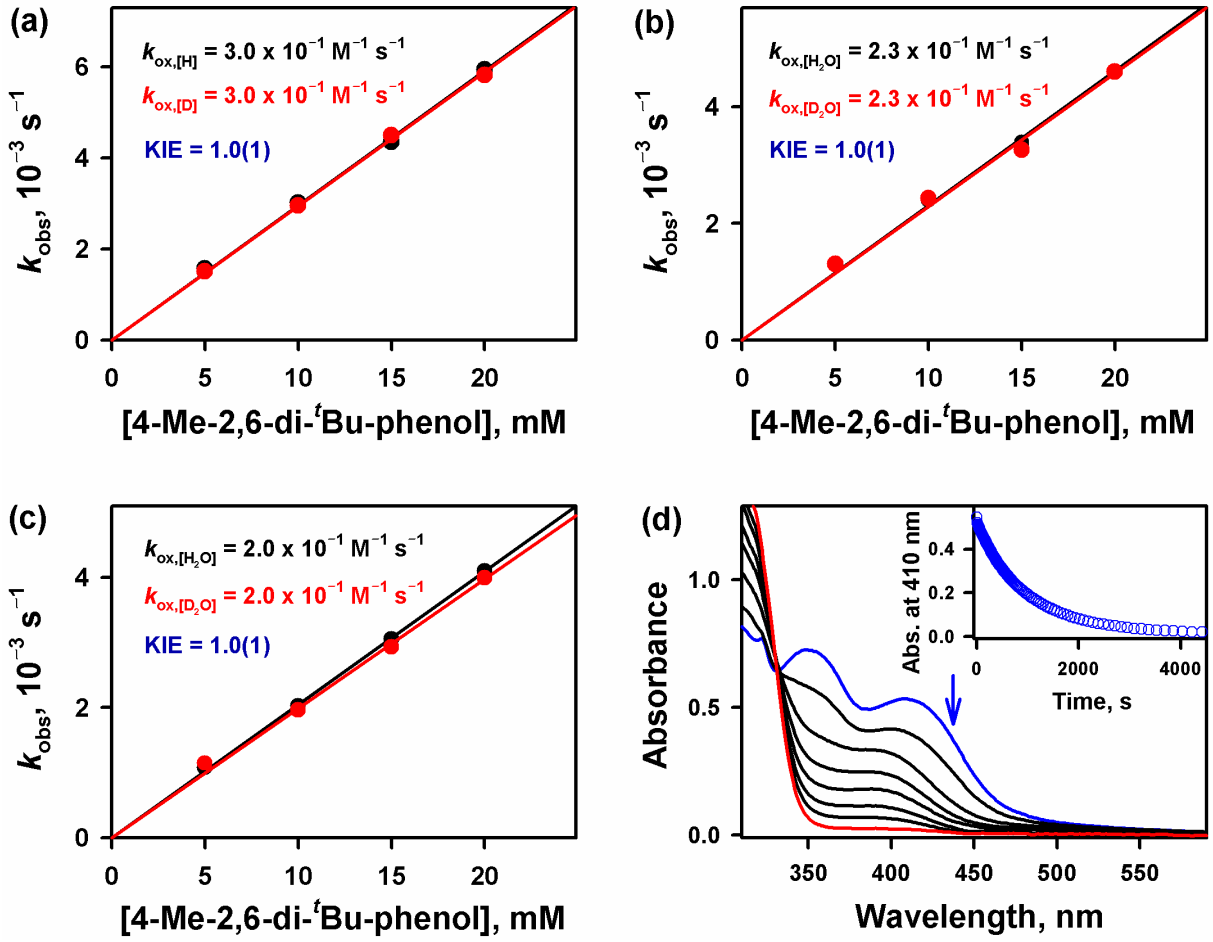

Figure S27. (a) Plot of pseudo-first-order rate constants against concentration of 4-methyl-2,6-di-*tert*-butylphenol obtained in the oxidation of 4-methyl-2,6-di-*tert*-butylphenol-*h* (black circles) and 4-methyl-2,6-di-*tert*-butylphenol-*d* (red circles) by **1** in MeCN at 298 K to determine the second-order rate constants (k_{ox}) and KIE values. (b, c) Plots of pseudo-first-order rate constants against concentration of 4-methyl-2,6-di-*tert*-butylphenol obtained in the oxidation of 4-methyl-2,6-di-*tert*-butylphenol by **1** in the presence of H_2O (black circles) and D_2O (red circles) [(b) 1.4 M and (c) 2.8 M] in MeCN at 298 K to determine the second-order rate constants (k_{ox}) and KIE values. (d) UV-visible absorption spectral changes observed in the oxidation of 4-methyl-2,6-di-*tert*-butylphenol (20 mM) by **1** (0.20 mM) in MeCN at 298 K. Inset shows time profile of the decay of absorbance at 410 nm due to **1**.

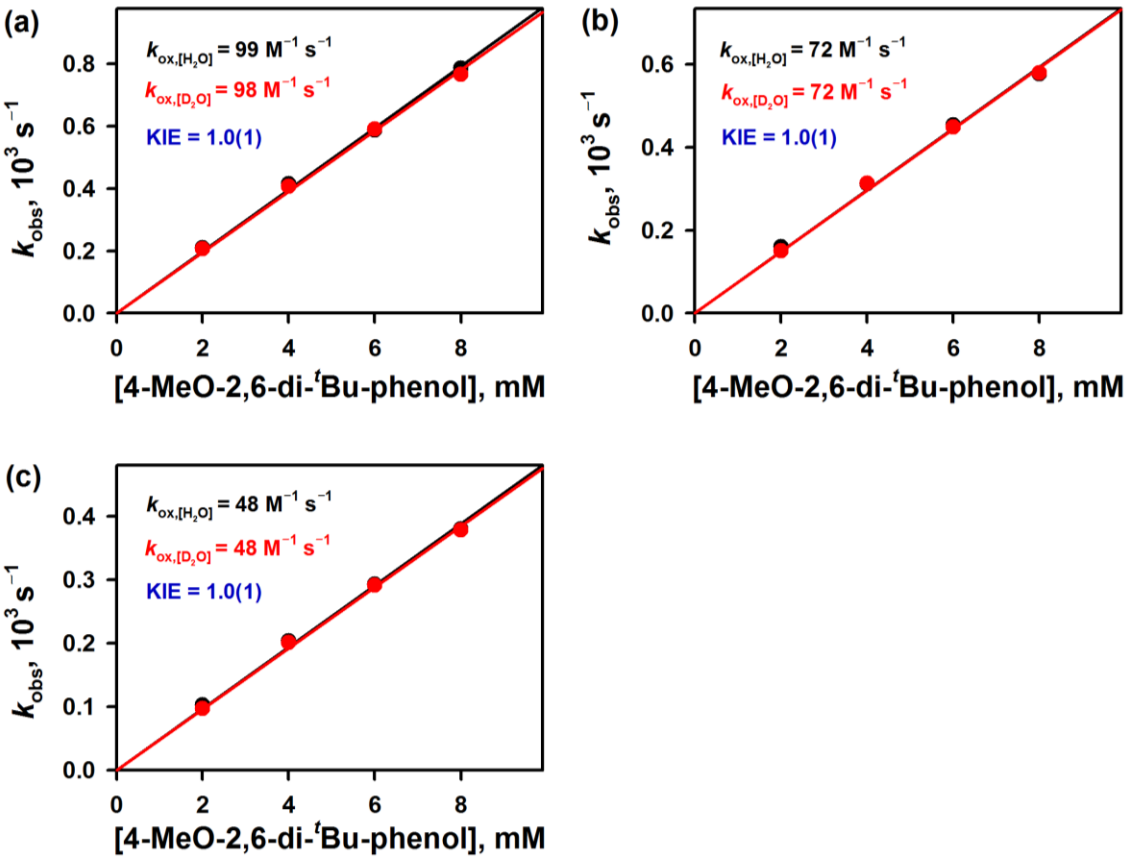

Figure S28. Plots of pseudo-first-order rate constants against concentration of 4-methoxy-2,6-di-*tert*-butylphenol obtained in the oxidation of 4-methoxy-2,6-di-*tert*-butylphenol by **1** in the presence of H_2O (black circles) and D_2O (red circles) [(a) 1.4 M, (b) 2.8 M and (c) 4.2 M] in MeCN at 298 K to determine the second-order rate constants (k_{ox}) and KIE values.

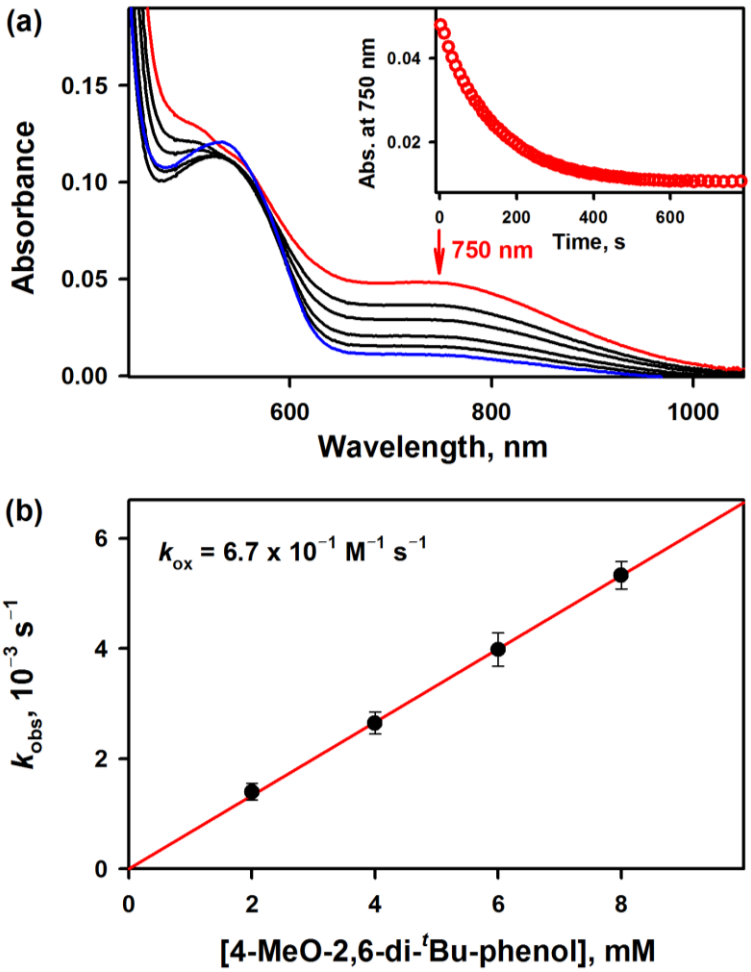

Figure S29. (a) UV-visible spectral changes observed in the oxidation of 4-methoxy-2,6-di-*tert*-butylphenol (8.0 mM) by **2** (0.40 mM; red line) in MeCN at 298 K. Inset shows time profile of absorbance at 750 nm due to **2**. (b) Plot of pseudo-first-order rate constants (k_{obs}) against concentration of 4-methoxy-2,6-di-*tert*-butylphenol obtained in the oxidation of 4-methoxy-2,6-di-*tert*-butylphenol by **2** in MeCN at 298 K to determine the second-order rate constant (k_{ox}).

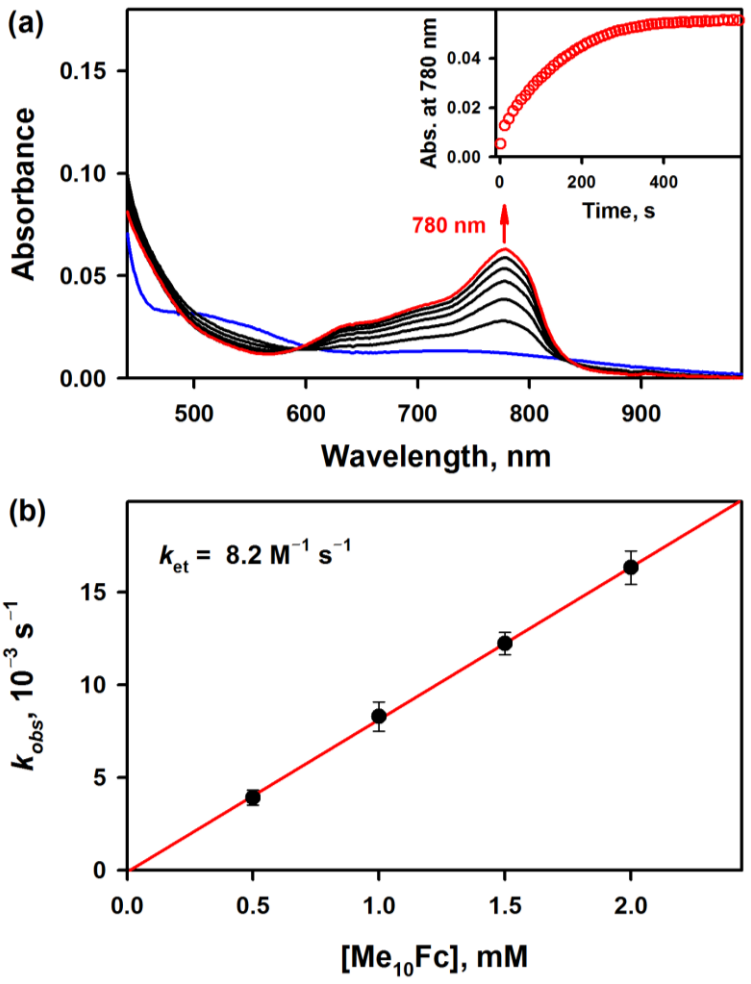

Figure S30. (a) UV-visible spectral changes observed in electron transfer from decamethylferrocene ($Me_{10}Fc$, 1.0 mM) to **2** (0.10 mM) in MeCN at 298 K. Inset shows time profile of absorbance at 780 nm due to decamethylferrocenium cation ($Me_{10}Fc^{+}$). (b) Plot of pseudo-first-order rate constants (k_{obs}) against concentration of $Me_{10}Fc$ obtained in electron transfer from $Me_{10}Fc$ to **2** in MeCN at 298 K to determine the second-order rate constant (k_{et}).

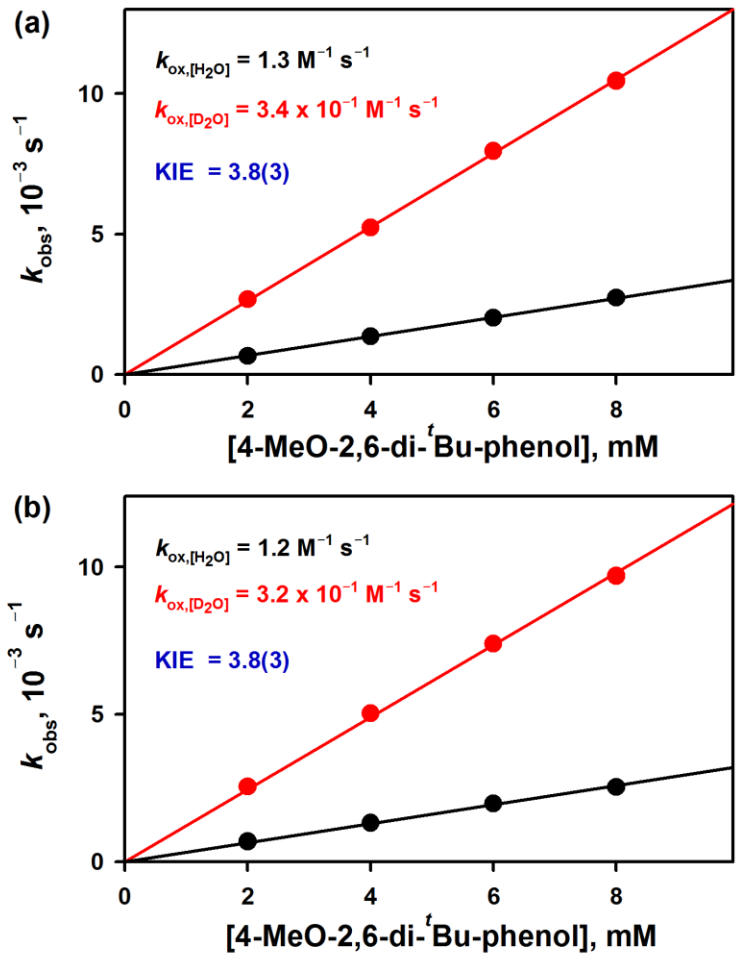

Figure S31. Plots of pseudo-first-order rate constants against concentration of 4-methoxy-2,6-di-*tert*-butylphenol obtained in the oxidation of 4-methoxy-2,6-di-*tert*-butylphenol by **2** in the presence of H_2O (black circles) and D_2O (red circles) [(a) 1.4 M and (b) 2.8 M] in MeCN at 298 K to determine the second-order rate constants (k_{ox}) and KIE values.

References

(S1) Armarego, W. L. F.; Chai, C. L. L. *Purification of Laboratory Chemicals*, 6th ed.; Pergamon Press: Oxford, 2009.

(S2) Dixon, N. E.; Lawrance, G. A.; Lay, P. A.; Sargeson, A. M.; Taube, H. *Inorg. Synth.* **1990**, *28*, 70.

(S3) Hitomi, Y.; Arakawa, K.; Funabiki, T.; Kodera, M. *Angew. Chem., Int. Ed.* **2012**, *51*, 3448.

(S4) (a) Sankaralingam, M.; Jeon, S. H.; Lee, Y.-M.; Seo, M. S.; Ohkubo, K.; Fukuzumi, S.; Nam, W. *Dalton Trans.* **2016**, *45*, 376. (b) Wijeratne, G. B.; Corzine, B.; Day, V. W.; Jackson, T. A. *Inorg. Chem.* **2014**, *53*, 7622.

(S5) Mann, C. K.; Barnes, K. K. *Electrochemical Reactions in Non-aqueous Systems*; Mercel Dekker: New York, 1970.

(S6) Sheldrick, G. M. in *SHELXTL/PC Version 6.12 for Windows XP*; Bruker AXS Inc.: Madison, Wisconsin, USA, 2001.

(S7) (a) Sankaralingam, M.; Lee, Y.-M.; Jeon, S. H.; Cho, K.-B.; Nam, W. *Chem. Commun.* **2018**, *54*, 1209. (b) Arunkumar, C.; Lee, Y.-M.; Lee, J. Y.; Fukuzumi, S.; Nam, W. *Chem.–Eur. J.* **2009**, *15*, 11482. (c) Goldsmith, C. R.; Jonas, R. T.; Stack, T. D. P. *J. Am. Chem. Soc.* **2002**, *124*, 83.

(S8) Muckerman, J. T.; Skone, J. H.; Ning, M.; Wasada-Tsutsui, Y. *Biochim. Biophys. Acta* **2013**, *1827*, 882.